Effects of α-crystallin gene knockout on zebrafish lens development

Mason Posner[1], Kelly L. Murray[1], Brandon Andrew[1], Stuart Brdicka[1], Alexis Butterbaugh-Roberts[1], Kirstan Franklin[1], Adil Hussen[1], Taylor Kaye[1], Emmaline Kepp[1], Mathew S. McDonald[1], Tyler Snodgrass[1], Keith Zientek[2] and Larry David[2]

[1]Department of Biology and Toxicology, Ashland University, Ashland, OH
[2]Department of Biochemistry and Molecular Biology, Oregon Health and Science University

Correspondence to:

Mason Posner
Ashland University, Department of Biology and Toxicology
401 College Avenue, Ashland, OH 44805
Phone: (419) 289-5691
email: mposner@ashland.edu

Abstract

The α-crystallin small heat shock proteins contribute to the transparency and refractive properties of the vertebrate eye lens and prevent the protein aggregation that would otherwise produce lens cataract, the leading cause of human blindness. There are conflicting data in the literature as to what role the α-crystallins may play in early lens development. In this study we used CRISPR gene editing to produce zebrafish lines with null mutations for each of the three α-crystallin genes (*cryaa*, *cryaba* and *cryabb*). Absence of protein was confirmed by mass spectrometry and lens phenotypes were assessed with differential interference contrast microscopy and histology. Loss of αA-crystallin produced a variety of lens defects with varying severity in larval lenses at 3 and 4 dpf, but little significant change in normal fiber cell denucleation. Loss of either αBa- or αBb-crystallin produced no significant lens defects. Mutation of each α-crystallin gene did not alter the expression levels of the remaining two, suggesting a lack of genetic compensation. These data confirm a developmental role for αA-crystallin in lens development, but the range of phenotype severity suggests its loss simply increases the chance for defect, and that the protein is not essential. Our finding that *cryaba* and *cryabb* null mutants lack noticeable lens defects is congruent with insignificant transcript levels in lens epithelial and fiber cells. Future experiments can explore the molecular consequences of *cryaa* mutation and causes of lens defects in this null mutant, as well as the roles of other genes in lens development and function.

Introduction

Alpha crystallins are small heat shock proteins that contribute to the high protein density that produces the refractive power of the vertebrate eye lens (Horwitz, 1992). Because of their ability to bind denaturing proteins and block aggregation, α-crystallins are thought to prevent lens cataract, the leading cause of human blindness worldwide. Their expression in tissues outside the eye, especially the broadly expressed αB-crystallin, also suggests that they may play diverse physiological roles (Srinivasan, Nagineni & Bhat, 1992). Numerous studies link αB-crystallin to the physiology and disease of muscular and nervous tissue (Bova et al., 1999).

Zebrafish have been a valuable model for investigating lens crystallin function. Zebrafish and human lenses are made of similar proteins, and the mechanisms underlying their development are conserved (Posner et al., 2008; Greiling, Aose & Clark, 2010). The production of large numbers of transparent embryos and the ease with which zebrafish can be genetically manipulated makes them a good tool for examining crystallin function. The presence of two αB-crystallin paralog genes in zebrafish provides an opportunity to dissect the roles of this multi-functional single mammalian protein (Smith et al., 2006). The accessibility of early-stage embryos and fast development times make zebrafish ideal for studying the roles of α-crystallins in early lens development. These studies in zebrafish are more convenient and much less costly than in mammalian systems such as mouse.

Various genetic knockout and translation blocking techniques have been used to investigate the impacts of α-crystallin loss on zebrafish lens development. These experiments showed that loss of any of the three α-crystallin genes produced lens defects in 3 and 4 day old fish (Zou et al., 2015; Mishra et al., 2018). This result differed from work in mouse, which showed that while the loss of αA-crystallin led to reduced lens size and early cataract development, the loss of αB-crystallin did not produce a lens phenotype, although heart defects were found (Brady et al., 1997, 2001). Furthermore, our recent analysis of zebrafish gene expression at single cell resolution indicated that neither of the two αB-crystallin genes were expressed in the lens at significant levels through five days of development (Farnsworth, Posner & Miller, 2021). Therefore, there seems to be conflicting reports on what role, if any, αB-crystallins play in early lens development.

In this present study we examine the larval lens in newly generated knockout lines for all three zebrafish α-crystallin genes. The resulting data address open questions about what effect, if any, the loss of either αB-crystallin protein will have on lens development. We also provide a more detailed analysis of lens phenotypes after αA-crystallin loss and compare several approaches for producing gene knockouts using CRISPR editing. This data analysis can provide a set of best practices for future studies of lens gene function.

Materials and Methods

Fish maintenance

The use of zebrafish in this study was approved by Ashland University's Animal Use and Care Committee (approval #MP 2019-1). Fish were maintained on a recirculating aquarium system at approximately 28°C with a 14:10 light and dark cycle with daily water changes. Juveniles and adults were fed twice each day with a combination of dry flake food and live *Artemia* cultures. Adults were bred in separate false bottom tanks to collect fertilized eggs, which were incubated in petri dishes with system water at 28°C. Resulting larvae that were to be raised to adulthood were fed a liquid slurry of ground zooplankton and green algae until large enough to eat flake food and *Artemia*.

Guide RNA design, production and injection

Target regions for the guide RNA (gRNA) used in single and double injections were identified using the CRISPR design tool in the *Benchling* digital notebook system (www.benchling.com). The target regions for the four-gRNA mix used with *cryaa* were identified by Wu et al. 2018 (Wu et al., 2018). Sequences for all gRNA primers are shown in Supplemental Table 1. Guide RNAs were produced using a PCR-based plasmid-free approach that annealed and elongated a universal scaffold primer with one, two or four additional primers containing the sequence of the target region. Equimolar amounts of universal scaffold primer and target region primers were used with Q5 DNA polymerase (NEB). Cycling parameters included a touchdown PCR protocol: initial 94°C denaturation for 5 min; cycle parameters: 94°C for 20 sec, 65° for 20 sec, 68°C for 15 sec (13 additional cycles with extension temperature reduced 0.5°C per cycle); 30 additional cycles of: 94°C for 20 sec, 58°C for 20 sec, 68°C for 15 sec; final extension 68°C for 5 minutes. Resulting PCR product was purified with the Monarch PCR and DNA Cleanup Kit (NEB) with elution in 20 microliters nuclease free water. Up to 1000 ng of purified PCR product was used with the HighScribe T7 kit (NEB) and incubated overnight at 37°C and reaction was purified with the Monarch RNA Cleanup Kit (500 micrograms) with elution in 50 μl nuclease free water (NEB). Quality of the gRNA prep was confirmed by agarose gel.

Each injection mix contained 250 ng/μl total of the purified gRNAs and 500 ng/μl of recombinant Cas9 protein (PNA Bio) with 0.2% phenol red in nuclease free water. One nanoliter of mix was microinjected with a single 20 millisecond pulse into the cytoplasm of each zebrafish zygote using a Harvard Apparatus PL-90 picoinjector (Holliston, MA).

Identification of null lines

Embryos injected with single or double gRNAs were genotyped after at least two months of age. Fish were anesthetized in 0.016% tricaine methane sulfonate (MS-222) resuspended in trisma base and the posterior edge of the fin was removed with scissors. Fish were kept separated for recovery and while genotyping took place. Genomic DNA was collected from each fin clip using the Monarch Genomic DNA Purification kit (New England Biolabs) and amplified with PCR primers that flanked the gRNA targeted region using OneTaq 2X Master Mix (NEB). The recommended PCR protocol was followed, with appropriate annealing temperatures determined experimentally. All primers and annealing temperatures are shown in Supplemental Table 1. Amplified genomic DNA targeted with one gRNA was sequenced to determine whether more than one sequence was apparent beginning at the target

area. Mutated genomic regions targeted with two gRNAs could be identified directly by the size of the resulting PCR product.

Fish resulting from injected zygotes (founder fish) determined through fin clipping to contain mutant alleles were outcrossed to wildtype fish. Ten resulting embryos were combined and homogenized to purify genomic DNA and the targeted gene region amplified to determine if the parent founder fish had passed on mutant alleles to offspring. If offspring were found to be heterozygous for a gene mutation, larvae were raised another two months for fin clipping. For single gRNA injected fish, sequencing of the heterozygotes was done to determine if the resulting mutation would cause a frame shift and early stop codon. Multiple heterozygotes with the same identified frame shift mutation were incrossed to produce null individuals that were then used to produce null lines. For double gRNA injected embryos, sequencing was used to identify heterozygotes with the same deletion, which were then incrossed to generate a null line.

Proteomic assessment of knockout fish

A detailed protocol outlining the sample preparation of zebrafish lenses to detect the presence of α-crystallins was previously published (Posner et al., 2017). Briefly, 50 µg portions of protein derived from either one or two dissected lenses were digested overnight with trypsin in the presence of ProteaseMax™ detergent as recommended by the manufacturer (ProMega, Madison, WI, USA). One µg of each tryptic digest was then injected at 10 µl/min onto a Symmetry C18 peptide trap (Waters Corporation, Milford, MA, USA) for 0-5 min using a 98% water, 2% acetonitrile (ACN), 0.1% formic acid mobile phase, then switched onto a 75 µm x 250 mm NanoAcquity BEH 130 C18 column (Waters Corporation) using mobile phases water (A) and ACN (B) each containing 0.1% formic acid, and peptides separated using a 7.5-30% ACN over 5-35 min, 30-98% from 35-36 min, 98% ACN from 36-41 min, 98-2% ACN from 41-42 min, and 2% ACN from 41-60 min at a 300 nL/min flow rate. Eluent was analyzed using a Q-Exactive HF mass spectrometer using electrospray ionization with a Nano Flex Ion Spray Source fitted with a 20 µm stainless steel nano-bore emitter spray tip and 1.0 kV source voltage (ThermoFisher Scientific, San Jose, CA, USA). Xcalibur version 4.0 was used to control the system. Survey mass spectra were acquired over m/z 400−1050 at 120,000 resolution, automatic gain control (AGC) target 3×10^6, maximum ion time (MIT) of 200 ms, profile mode, and lock mass correction using m/z = 445.12002 and 391.28429 polysiloxane ions. Parallel reaction monitoring (PRM) was also performed using a list of 39 precursors from αA, αBa, and αBb zebrafish crystallin peptides, as well as α-spectrin to assess column loading. A loop count was set to repeat precursor scans every 10 PRM scans. PRM scans were performed at 15,000 resolution, AGC target 2×10^5, MIT of 100 ms, normalized collision energy of 27, and isolation width of 2 m/z. Results were processed using Skyline Software version 21.1.0.278 (Pino et al., 2020) using a previously constructed spectral library generated by a data-dependent MS/MS experiment from a wild type zebrafish lens digest (Posner et al., 2017). The relative abundance was determined by comparison of 4 peptides with the strongest intensities from each of the proteins. (Peptides and precursor masses listed in Supplemental Table 2).

Phenotype assessment

Embryos produced by incrossing the null lines were treated in 0.2 mM PTU in system water between 6 and 20 hours post fertilization to maintain transparency. The gross anatomy of each larva was imaged at 45 total magnification on a dissecting microscope while one of their lenses was imaged at 200X total

magnification using differential interference microscopy on an Olympus IX71 microscope. Images were taken with SPOT cameras and were cropped and oriented using ImageJ (NIH). Lens diameters were measured in ImageJ with a line spanning the lens equator, which differs from the anterior-posterior dimension (Wang et al., 2020). Body lengths were measured from the tip of the snout to the end of the axial skeleton. Any statistically significant differences in measurements between genotypes was calculated using the *anova* and *TukeyHSD* functions in R (R Core Team, 2021) within RStudio (RSTudio Team, 2020).

Larvae were anesthetized and then transferred to 4% paraformaldehyde with 5% sucrose for storage at 4°C until cryosectioning and DAPI staining to observe the presence of lens cell nuclei. The sectioning procedure has been previously reported (Posner et al., 2013). Resulting slides with 10 micron lens sections were mounted using Vectashield Antifade Mounting Medium with DAPI (Vector Laboratories) and imaged on an Olympus IX71 microscope. DAPI intensity across the diameter of the lens was measured using the Concentric Circles plugin for ImageJ. An oval was drawn matching lens shape and 10 concentric circles were used to quantify average pixel intensity along the perimeter of each circle. Any statistically significant differences in average pixel intensity between genotypes at each circle was calculated with a Mann-Whitney U test in R. All scripts and data used for this and other analyses in this study can be found in this repository on GitHub: github.com/masonfromohio/alpha-crystallin-CRISPR-Rscripts

Quantitative PCR analysis of alpha crystallin expression

The qPCR methods were designed to meet MIQE guidelines (Bustin et al., 2009) and followed methods previously described (Posner et al., 2017). Larvae were collected at 7 dpf and stored in RNAlater (Thermo) at 4°C for up to one month until used for purification of total RNA with the Monarch Total RNA Miniprep Kit (NEB). Five larvae were used for each RNA purification and homogenized in DNA/RNA protection buffer with a glass homogenizer prior to proteinase K digestion, following the kit protocol. DNase treatment was performed in the RNA purification column, with a final elution in 50 µl of nuclease free water. The concentration of collected RNA was measured in a Nanodrop One (Thermo Fisher). The ProtoScript II First Strand cDNA Synthesis Kit (NEB) was used with 600 ng of total RNA from each sample with the d(T)23 VN primer using the standard protocol and -RT controls were included.

Luna Universal qPCR Master Mix (NEB) was used to amplify 1.5 µl of each cDNA sample in a 20 µl total reaction using the manufacturer's standard protocol on an Applied Biosystems StepOne Real-Time PCR System (Thermo). Three technical replicates were used for each cDNA sample, while two technical replicates were used with all -RT and non template controls (water). Two endogenous control primer sets were included (*rpl13a* and *ef1a*). All primer sequences and previously calculated efficiencies are shown in Table 2 of (Posner et al., 2017). Reactions included primers at a final concentration of 250 nm with the following parameters: hold at 95°C for 1 min; 40 cycles of 95°C for 15 s and 60°C for 30 s; fast ramp setting. Melt curve analysis was used to confirm that single products were produced, and amplification products had previously been sequenced to confirm their expected identity (Posner et al., 2017). Analysis of resulting Cq values was identical to the process previously reported (Posner et al., 2017).

Results

Disruption of cryaa *produced several types of lens defects that ranged in severity*

We used two approaches to mutate the zebrafish *cryaa* gene to prevent the production of αA-crystallin protein. First, we injected a single guide RNA (gRNA) to produce frame shift mutations and an early stop codon (Fig 1A). This approach successfully produced a 5 base pair deletion and early stop codon after the leucine residue in position 27 (Fig 1B). Mass spectrometry confirmed that this mutant prevented the production of any measurable αA-crystallin protein, as shown by the absence of αA-crystallin peptide 52-65 in the *cryaa* -/- lens (Fig 1C, right). Three additional αA-crystallin peptides that were monitored were also missing in *cryaa* -/- lens (Supplemental Fig. 3B-D). Differential interference contrast (DIC) microscopy of anesthetized and PTU treated larvae at 3 days post fertilization (dpf) showed that *cryaa* homozygous null fish (cryaa$^{-/-}$) had lens irregularities. These phenotypes included a central roughness and disorganization of central fiber cells compared to wildtype controls (Fig 1 D-F). Because this original *cryaa* null line stopped breeding, we produced a second null line by using two gRNAs to produce an 863 bp deletion that removed a portion of the *cryaa* promoter and start codon region (Fig 2A). This approach made it simpler to identify mutants by PCR (Fig 2B) and reduced the potential for genetic compensation due to mutant mRNA degradation, as no truncated mRNA would be produced (El-Brolosy et al., 2019). The resulting *cryaa* null line bred well and all further data presented are from these fish.

A significant proportion of *cryaa* null larvae had lenses that appeared similar to those of wildtype fish (Fig 2C). Others showed phenotypes that we classified into five categories. Some lenses had central roughness that appeared as many small darker spots in the region of the primary fiber cells (Fig 2D). Some lenses contained elongated roughened areas that appeared to trace the edges of fiber cell boundaries (Fig 2 D and E, black arrows). We also found lenses with a disorganization of central fiber cells (Fig 2 E and F). These lenses did not show the regular circular rings of central fiber cells. Some lenses showed more severe boundaries between fiber cells, possibly at the interface between the lens nucleus and cortex (Fig 2G, black arrows), and some lenses exhibited large pits (Fig 2H).

Frame shift mutations of the two paralogs for zebrafish αB-crystallin genes did not produce noticeable lens defects

Single gRNAs were designed to target exon 1 in both the *cryaba* and *cryabb* genes (Fig 3). Injected embryos were raised and those with mutations leading to frameshifts and early stop codons were identified. A single basepair deletion in *cryaba* led to altered amino acid sequence after residue 14 and a stop codon at residue 65 (Fig 3B). Mass spectrometry indicated that lenses from *cryaba* homozygous mutant adults expressed no detectable αBa-crystallin, as evidenced by missing tryptic peptide 11-21 in the mutant lens (Fig 3C, right). An 8 bp deletion in *cryabb* produced altered amino acids after residue 9 and a stop codon at residue 26 (Fig 3D & E). Digests of adult *cryabb* homozygous null fish lens had undetectable levels of peptide 45-57 (Fig 3F, right). While minor amounts of other *cryaba* and *cryabb* peptides from null fish lenses were sometimes detected, these were attributed to carry-over on the liquid chromatography column from prior analysis of wildtype lenses (Supplemental Fig. 1: G-I and J-L).

The prevalence of lens defects in larvae generated by our *cryaa*, *cryaba* and *cryabb* null lines was quantified at 3 and 4 dpf to assess the impacts of loss of each α-crystallin on lens development (Fig 4). The least common defect, but a characteristic one in *cryaa* null larvae, was the presence of visual roughness in the center of the lens. A more common defect, but most prevalent after *cryaa* loss, was a defect seen in peripheral fiber cells that appeared as a widening of the normally tight boundary between these cells. This peripheral fiber cell defect was more common at 4 dpf in both *cryaa* null larvae and larvae directly observed after injecting embryos with a four-guide RNA mix (pgRNA). Two other defect types: a disorganization of central lens and severe boundaries between fiber cells, all occurred in some wildtype lenses, but were more common in *cryaa* homozygous null larvae. Pitting in the lens was the most common defect seen in wildtype larvae and not noticeably increased after *cryaa* loss. All defect types were seen in *cryaba* and/or *cryabb* null larvae, but at much reduced proportions compared to *cryaa* null larvae, and at levels similar to wildtype larvae. When pooling all defects together, over 60% of *cryaa* null larvae showed some defect, whereas *cryaba* and *cryabb* null larvae showed below 20%, similar to wildtype larvae.

All larvae used to assess lens phenotype were measured to record body length and lens diameter at 3 and 4 dpf (Fig 5). These data show an increase in body length from 3 to 4 dpf in all genotypes, as would be expected. Body length was more varied between two independent wildtype samples than between wildtype and null samples, suggesting that gene knockout did not alter overall fish growth rate compared to wildtypes. There appeared to be little to no difference in lens diameter between 3 and 4 dpf samples, which produced a decrease in the lens to body length ratio between those two timepoints for all genotypes. The only measurement that was statistically different from both wildtype samples was the lens diameter of *cryabb* knockout larvae at 4 dpf.

Loss of α-crystallins did not disrupt fiber cell denucleation

Fiber cells of the zebrafish lens elongate and lose their nuclei between 2 and 3 dpf. We examined lenses histologically at 3 and 4 dpf to determine if this process was altered by loss of each α-crystallin (Fig 6). Wildtype lenses showed that the details of this process can vary, but that the majority of lenses have cleared all nuclei from central fiber cells, leaving elongated nuclei at the posterior margin (Fig 6A, white boxes). We consistently found two posterior zones of extended fiber cells bordering a denucleated space between them (Fig 6A, asterisk), with what appeared to be a single layer of nuclei adjacent to the retinal neurons. Lenses contained rings of DAPI staining just anterior to the remaining, elongated fiber cells and extending forward with a gap between the anterior margin and the epithelial fiber cells (Fig 6A, white arrows). The posterior-most gap between elongated fiber cells was a good indicator that sections imaged were through the equator of the lens. Elongated fiber cell nuclei in wildtype lenses ranged from flat to wavy, and occasionally retained an oval shape (Fig 6C, white arrow). At 4 dpf the posterior fiber cell nuclei stacks appeared thinner and the DAPI rings less common.

The lenses of *cryaa* null 3 dpf larvae also varied in phenotype. However, more abnormal phenotypes were seen. A small number of *cryaa* null lenses retained fiber cell nuclei deep to the central DAPI staining ring (Fig 6 I and J) or on the ring itself (Fig 6H). Quantitation of pixel intensity also showed that some *cryaa* null larval lenses had higher amounts of DAPI staining material in the deeper parts of the cortex and lens nucleus, but the mean pixel intensity did not differ statistically from wildtype larvae (Fig 6N). None of the 4 dpf *cryaa* null larvae examined retained abnormal fiber cell nuclei. None of the

cryaba or *cryabb* 3 dpf larvae examined showed retained fiber cell nuclei within the central lens (Supplemental Figure 2). However, some lenses did appear to have thicker fiber cell nuclei stacks, and possibly more oval nuclei, although these features were also seen in some wildtype lenses as described above.

CRISPR deletion of each α-crystallin gene did not alter expression of the other two

Quantitative PCR (qPCR) was used to measure α-crystallin gene expression levels in wildtype and our knockout lines. This allowed us to determine if mutation led to a decrease in mRNA levels for the damaged gene or changes in expression of the other α-crystallin genes. Whole larvae were assessed at 7 dpf as earlier work showed low levels of *cryaba* and *cryabb* expression through 4 and 5 dpf, respectively (Posner et al., 2017), and almost no expression in the lens (Farnsworth, Posner & Miller, 2021). We found reduced levels of *cryaa* mRNA in 7 dpf homozygous null mutants with the large deletion removing the proximal promoter and start codon (Fig 7A). Expression levels of *cryaa* did not increase in *cryaba* and *cryabb* null larvae compared to wildtype larvae (Fig 7A). The *cryaba* and *cryabb* null lines were not produced by deleting the promoter and start codon, but instead were produced with a single gRNA producing frame shift mutations and early stop codons (Fig 3). *cryaba* mRNA levels were not different in the *cryaba* null larvae compared to wildtype, nor were they increased in the other null lines (Fig 7B). Messenger RNA for *cryabb* was reduced in *cryabb* null larvae compared to other mutant lines (Fig 7C). While delta Cq values for *cryabb* mRNA in *cryabb* null mutants were all lower than wildtype larvae, this difference was not statistically significant. Messenger RNA levels for *cryabb* were not statistically significantly increased in *cryaa* or *cryaba* null mutants compared to wildtype larvae.

Discussion

We produced mutant zebrafish lines lacking each of the three α-crystallin proteins. Lack of αA-crystallin caused a variety of visible lens defects in mutant larvae not seen, or present at lower frequency, in wildtype larvae. Lack of either αB-crystallin did not cause an increase in lens abnormalities. Loss of αA-crystallin did not alter overall lens growth, nor significantly disrupt the fiber cell denucleation important for lens development. Finally, none of the gene knockouts produced compensatory changes in mRNA levels of the others. These data suggest that loss of αA-crystallin makes zebrafish lenses more susceptible to defects in development, but does not always trigger these defects. Loss of either *cryaba* nor *cryabb* produced no noticeable changes in lens development through four days of development.

Our observation of lens abnormalities in our CRISPR-produced *cryaa* null larvae matches previous work done with a TALEN-produced *cryaa* knockout line (Zou et al., 2015). Lens images from that study showed central roughness and pitting of the lens, but not the central disorganization, peripheral fiber cell defects or severe fiber cell boundaries that we found to be characteristic of *cryaa* null larvae. The proportion of null incross larvae with lens defects in the TALEN study was approximately 85%, a bit more than our finding of 60%. However, that study separated their phenotypes into “minor” and “major”, with just over 40% of larvae with minor lens defects. Despite the different methods used to characterize lens defects in our present study and this past TALEN work, it seems that the observed

penetrance of *cryaa* loss is comparable. It is notable that the effects of αA-crystallin loss can range from no apparent defect in lens structure to a variety of defects that can occur singly or in combination. A similar range in lens effects was seen after CRISPR knockout of zebrafish aquaporin 0 paralogs, *mipa* and *mipb* (Vorontsova et al., 2018). Our results suggest that αA-crystallin is not essential for proper lens development through 4 days post fertilization, but that its loss does predispose the lens to defect. The only other model species with an αA-crystallin knockout line is the mouse (Brady et al., 1997). Due to the *in utero* development of the mouse, and its pigmentation, it was likely not feasible to make similar observations of lens development at comparable stages to this study. However, that study showed that *cryaa* null mice develop cataract by 7 weeks of age, indicating the protein's importance in lens biology. The impact of *cryaa* loss on zebrafish lens clarity as animals age can be addressed in the future using our validated lines.

The results of CRISPR null mutation, reported here, can be compared to prior knockdowns by morpholino injection. We previously reported a lack of lens defects in zebrafish larval lenses at 3 dpf after using a morpholino to block the translation of αA-crystallin (Posner et al., 2013). Similar results were reported in a later study (Hinaux et al., 2014). Neither study imaged lenses using DIC microscopy, so it is possible that defects like those identified in this current study were missed. It is also possible that small amounts of αA-crystallin produced during those morpholino experiments were sufficient to prevent the defects found in this study.

Our data do not directly address mechanisms behind the lens defects seen in our *cryaa* null lenses. Histology and DAPI staining of 3 and 4 dpf larvae indicate that while there may be some delay in fiber cell denucleation in *cryaa* null lenses, this was found in a small proportion of lenses at 3 dpf and gone by 4 dpf. Because αA-crystallin has documented functions as an anti-aggregation chaperone that can buffer the effects of stress in the lens (Horwitz, 1992), it is possible that its loss may make the lens more susceptible to protein aggregation. This likely led to the cataract seen in *cryaa* null mouse lenses (Brady et al., 1997), and since zebrafish αA-crystallin has chaperone activity (Dahlman et al., 2005; Koteiche et al., 2015), aggregates in central fiber cells may lead to observed central roughness. This hypothesis could be tested by future proteomic analysis of insoluble protein. Other defects we observed hint at a breakdown in normal fiber cell arrangement. Under DIC imaging the fiber cell borders in the zebrafish lens are visible as regular concentric rings (Fig 1D). Our observation of central disorganization suggests defects in this cellular arrangement affecting central fiber cells. A separate defect produced short regions of expanded space between peripheral fiber cells, while least common were more severe, extended borders between fiber cells. These three anatomical defects were visually distinct, and may stem from different mechanistic defects in fiber cell interactions. It has been proposed that αA-crystallin may play a direct role in fiber cell differentiation (Boyle & Takemoto, 2000). While our *cryaa* null larvae did not show extended defects in fiber cell nucleus degradation, there may be other aspects of fiber cell differentiation impacted by αA-crystallin loss.

Our finding that lens diameters in *cryaa* null lenses at 3 and 4 dpf were similar to wildtype larvae matches results of a previous knockout study (Zou et al., 2015). Our *cryaba* and *cryabb* null larvae also appeared similar in body length and lens diameter to wildtype larvae. We included two separate samples of wildtype larvae to assess possible variation between breedings or different fish tanks with

the same genotype. The statistically significant variation in body length between these two wildtype samples suggests that variation between groups can be high, and should be taken into account when looking for changes in lens growth resulting from gene knockout. The observation that lens diameter was essentially unchanged between 3 and 4 dpf, while body length increased, was unexpected considering that past studies have found linear relationships between lens diameter and body length, although these studies did not examine fish prior to 7 dpf (Collery et al., 2014; Wang et al., 2020). It is possible that in these earlier stages body length and lens diameter growth are not parallel.

We found no evidence that mutation of either αB-crystallin gene in zebrafish caused abnormalities in lens development or structure. Neither our *cryaba* nor *cryabb* null mutant larvae showed any of the lens defects above levels seen in wildtype, with the exception of a few more larvae with peripheral fiber cell defects or severe fiber cell boundaries (Fig 4). This was in contrast to much higher proportions of all defects, except pitting, in *cryaa* null larvae. Fiber cell denucleation also appeared normal in both αB-crystallin mutant lines. The lack of developmental lens defects in these fish is consistent with knockout studies in mouse in which loss of the single αB-crystallin gene had no effect on lens clarity through 39 weeks of age, although early developmental stages were not examined (Brady et al., 2001). However, previously published CRISPR mutants for *cryaba* and *cryabb* did produce lens defects at 4 dpf in a large proportion of larvae (Mishra et al., 2018). In that study approximately 75% and 50% of *cryaba* and *cryabb* null larvae, respectively showed lens abnormalities. Defects were categorized as “minor” and “major” with little description of defect type. Two published images of lenses from a *cryaba* heterozygote cross show roughness or pitting as well as some gaps between fiber cells. Previous work by the same lab identified far more severe lens defects in zebrafish larvae after injection of translation-blocking morpholinos targeting *cryaba* and *cryabb* (Zou et al., 2015). However, general gross defects in resulting larvae suggest general toxicity from the morpholinos and not a lens specific effect. In their more recent CRISPR lines there were no reported general larval defects, further suggesting that the morpholino-induced lens defects were not specifically due to the loss of αB-crystallin proteins.

Existing data suggest that neither *cryaba* nor *cryabb* are significantly expressed in the zebrafish lens through 5 dpf, based on shotgun proteomics (Greiling, Houck & Clark, 2009) and single cell RNA-Seq (Farnsworth, Posner & Miller, 2021). These previous findings might explain the lack of noticeable early lens phenotypes in our αB-crystallin homozygous null larvae. The reason for the discrepancy in our present CRISPR work and a past study (Mishra et al., 2018) is unclear. Our mass spectrometry data indicated a loss of αBa- and αBb-crystallin in our null adult lenses, so our lack of a phenotype does not appear to be the result of residual protein. We did detect some residual peptides from these crystallins during our analysis, but these were attributed to carry over on the chromatography column during the highly sensitive parallel reaction monitoring analysis. It is possible that the difference in results is due to variation in the background genetics of the zebrafish lines used. We show in this study that different populations of wildtype fish can produce larvae with different lengths and lens diameters (Fig 5), and we see variable, low levels of lens defects in wildtype larvae between breedings. This variation could contribute to differences between studies.

The variety of approaches used to produce αA-crystallin mutants in this study allows us to compare their utility for studying resulting phenotypes. The quickest way to screen genes for their role in

development is to directly examine larvae injected at the zygote state. There is good evidence that this approach is effective when injecting a mix of four gRNAs (Wu et al., 2018). In our own hands we found this approach effective when targeting genes already known to play an essential role in lens development. For example, injection of a four gRNA mix (pgRNA) targeting the transcription factor *foxe3* closely replicated phenotypes reported in a stable zebrafish null line (Supplemental Fig 1; (Krall & Lachke, 2018)). However, when targeting *cryaa* this approach did not produce similar levels of phenotypes seen in our null line (Fig 4). The proportion of each defect differed between the two approaches, and the levels of some defects also differed between 3 and 4 dpf. These variations in phenotype could be due to the mosaic nature of gRNA injected larvae, in which some lens cells contain mutant *cryaa* alleles and others contain wildtype alleles. The expression of αA-crystallin in unaffected cells may be enough to prevent the defects seen in our null line. We previously showed that adult zebrafish lenses produce less αA-crystallin than mammalian lenses (Posner et al., 2008), and our past qPCR and single cell RNA-Seq data suggest that lens *cryaa* expression through 5 dpf is relatively low as well (Posner et al., 2017; Farnsworth, Posner & Miller, 2021). Since the complete loss of αA-crystallin in our *cryaa* null line only led to visible defects in 60% of larvae, the expression of reduced amounts in our injected embryos may be sufficient to alter the phenotype. It is also possible that differences are simply due to the stochastic nature of phenotype development. Considering the dynamic changes occurring in the zebrafish lens between 3 and 4 dpf it is best to quantify phenotypes for each day separately in future studies.

Because our initial *cryaa* null line generated with a single gRNA and containing a frame shift mutation stopped breeding, we took the opportunity to generate a second null line with a large deletion removing the proximal promoter region and start codon. Both lines generated similar lens defects, reinforcing the conclusion that these defects resulted from the loss of αA-crystallin and not off-target effects. There are two other benefits to generating mutant knockout alleles by deletion. First, these deletion alleles are simpler to screen, as they are identifiable by PCR without subsequent sequencing. Second, deletion of the promoter and start codon reduces the chance of possible genetic compensation after nonsense mediated mRNA decay (El-Brolosy et al., 2019). The loss of the targeted gene's mRNA can also be monitored by qPCR (Fig 7). Our two αB-crystallin null lines were produced with single gRNAs and frame shift mutations. While our proteomics work confirmed loss of each protein in our null adult fish lenses, qPCR showed reduction in *cryabb* mRNA in the *cryabb* null line, but no reduction in *cryaba* mRNA in the *cryaba* null line. This difference may reflect the unpredictability of non-sense mediated decay, and shows that mRNA levels do not necessarily reflect eventual protein levels. It is also possible that this difference in mRNA levels reflects primer location, as our *cryaba* qPCR primers annealed within exon 1, just downstream of the gRNA target site, while our *cryabb* primers annealed to the 5' UTR.

Several key questions remain unanswered in this study. It is unclear how the loss of αA-crystallin leads to the visual defects observed by DIC microscopy. Lenses from mutant and knockout α-crystallin mice have been analyzed by proteomics and RNA-Seq to identify changes in global gene expression (Andley et al., 2013, 2018). A similar approach would be valuable with our zebrafish null lines. We have only presented data through 7 dpf. It will be interesting to see how αA-crystallin loss impacts lens clarity and optics as fish age. While we know that both αB-crystallin genes are expressed in the adult lens, we

467 do not know at what age this expression begins, and how αB-crystallin loss may impact lenses as they
468 age. This question is particularly interesting as *cryaba* is lens specific in adults while *cryabb* is expressed
469 broadly, suggesting an ontogenetic shift in the function of these genes and their proteins. Why *cryaba*
470 is expressed outside the lens in early development, and whether it or *cryabb* plays an important
471 developmental role in those extralenticular tissues, is also unknown. Answers to these questions would
472 add to the understanding of why these small heat shock protein genes were co-opted as key players
473 during vertebrate lens evolution.
474
475
476 **Acknowledgements**
477
478 We would like to thank the many members of the zebrafish research community who were helpful
479 with technical suggestions. The plasmid-free protocol used to generate gRNAs was shared with us by
480 Dr. Cody Smith at the University of Notre Dame. Dr. Jennifer Phillips at the University of Oregon first
481 suggested our double gRNA deletion approach for generating our *cryaa* mutant. Caitlin Puff
482 contributed to the measurements of larval body length and lens diameters. This work was supported
483 by the NIH National Eye Institute (R15 EY13535) to MP, by the Provost Office at Ashland University's
484 (AU) student research grant program and by the AU Choose Ohio First program that provided summer
485 research support to KM. Mass spectrometric analysis was supported by the NIH National Institute (P30
486 EY010572.
487
488

Citations

Andley UP, Malone JP, Hamilton PD, Ravi N, Townsend RR. 2013. Comparative Proteomic Analysis Identifies Age-Dependent Increases in the Abundance of Specific Proteins after Deletion of the Small Heat Shock Proteins αA- and αB-Crystallin. *Biochemistry* 52:2933–2948. DOI: 10.1021/bi400180d.

Andley UP, Tycksen E, McGlasson-Naumann BN, Hamilton PD. 2018. Probing the changes in gene expression due to α-crystallin mutations in mouse models of hereditary human cataract. *PLoS ONE* 13:e0190817-18. DOI: 10.1371/journal.pone.0190817.

Bova MP, Yaron O, Huang Q, Ding LL, Haley DA, Stewart PL, Horwitz J. 1999. Mutation R120G in alphaB-crystallin, which is linked to a desmin-related myopathy, results in an irregular structure and defective chaperone-like function. *Proceedings of the National Academy of Sciences of the United States of America* 96:6137–6142.

Boyle DL, Takemoto LJ. 2000. A possible role for alpha-crystallins in lens epithelial cell differentiation. *Molecular vision* 6:63–71.

Brady JP, Garland D, Duglas-Tabor Y, Robison WG, Groome A, Wawrousek EF. 1997. Targeted disruption of the mouse alpha A-crystallin gene induces cataract and cytoplasmic inclusion bodies containing the small heat shock protein alpha B-crystallin. *Proceedings of the National Academy of Sciences of the United States of America* 94:884–889.

Brady JP, Garland DL, Green DE, Tamm ER, Giblin FJ, Wawrousek EF. 2001. AlphaB-crystallin in lens development and muscle integrity: a gene knockout approach. *Investigative ophthalmology & visual science* 42:2924–2934.

Bustin SA, Benes V, Garson JA, Hellemans J, Huggett J, Kubista M, Mueller R, Nolan T, Pfaffl MW, Shipley GL, Vandesompele J, Wittwer CT. 2009. The MIQE guidelines: minimum information for publication of quantitative real-time PCR experiments.

Collery RF, Veth KN, Dubis AM, Carroll J, Link BA. 2014. Rapid, Accurate, and Non-Invasive Measurement of Zebrafish Axial Length and Other Eye Dimensions Using SD-OCT Allows Longitudinal Analysis of Myopia and Emmetropization. *PLoS ONE* 9:e110699. DOI: 10.1371/journal.pone.0110699.

Dahlman JM, Margot KL, Ding L, Horwitz J, Posner M. 2005. Zebrafish alpha-crystallins: protein structure and chaperone-like activity compared to their mammalian orthologs. *Molecular vision* 11:88–96.

El-Brolosy MA, Kontarakis Z, Rossi A, Kuenne C, Günther S, Fukuda N, Kikhi K, Boezio GLM, Takacs CM, Lai S-L, Fukuda R, Gerri C, Giraldez AJ, Stainier DYR. 2019. Genetic compensation triggered by mutant mRNA degradation. *Nature*:1–26. DOI: 10.1038/s41586-019-1064-z.

Farnsworth D, Posner M, Miller A. 2021. Single cell transcriptomics of the developing zebrafish lens and identification of putative controllers of lens development. *Experimental Eye Research*:108535. DOI: 10.1016/j.exer.2021.108535.

Greiling TMS, Aose M, Clark JI. 2010. Cell fate and differentiation of the developing ocular lens. *Investigative ophthalmology & visual science* 51:1540–1546. DOI: 10.1167/iovs.09-4388.

Greiling TMS, Houck SA, Clark JI. 2009. The zebrafish lens proteome during development and aging. *Molecular vision* 15:2313–2325.

Hinaux H, Blin M, Fumey J, Legendre L, Heuzé A, Casane D, Rétaux S. 2014. Lens defects in Astyanax mexicanusCavefish: Evolution of crystallins and a role for alphaA-crystallin. *Developmental neurobiology*:n/a-n/a. DOI: 10.1002/dneu.22239.

Horwitz J. 1992. Alpha-crystallin can function as a molecular chaperone. *Proceedings of the National Academy of Sciences of the United States of America* 89:10449–10453.

Koteiche HA, Claxton DP, Mishra S, Stein RA, McDonald ET, McHaourab HS. 2015. Species-Specific Structural and Functional Divergence of α-Crystallins: Zebrafish αBa- and Rodent αA ins-Crystallin Encode Activated Chaperones. *Biochemistry* 54:5949–5958. DOI: 10.1021/acs.biochem.5b00678.

Krall M, Lachke SA. 2018. A zebrafish model of foxe3 deficiency demonstrates lens and eye defects with dysregulation of key genes involved in cataract formation in humans. *Human genetics* 137:315–328. DOI: 10.1007/s00439-018-1884-1.

Mishra S, Wu S-Y, Fuller AW, Wang Z, Rose KL, Schey KL, McHaourab HS. 2018. Loss of αB-crystallin function in zebrafish reveals critical roles in the development of the lens and stress resistance of the heart. *The Journal of biological chemistry* 293:740–753. DOI: 10.1074/jbc.m117.808634.

Pino LK, Searle BC, Bollinger JG, Nunn B, MacLean B, MacCoss MJ. 2020. The Skyline ecosystem: Informatics for quantitative mass spectrometry proteomics. *Mass Spectrometry Reviews* 39:229–244. DOI: 10.1002/mas.21540.

Posner M, Hawke M, Lacava C, Prince CJ, Bellanco NR, Corbin RW. 2008. A proteome map of the zebrafish (Danio rerio) lens reveals similarities between zebrafish and mammalian crystallin expression. *Molecular vision* 14:806–814.

Posner M, Murray KL, McDonald MS, Eighinger H, Andrew B, Drossman A, Haley Z, Nussbaum J, David LL, Lampi KJ. 2017. The zebrafish as a model system for analyzing mammalian and native α-crystallin promoter function. *PeerJ* 5:e4093-27. DOI: 10.7717/peerj.4093.

555 Posner M, Skiba J, Brown M, Liang JO, Nussbaum J, Prior H. 2013. Loss of the small heat shock protein
556 αA-crystallin does not lead to detectable defects in early zebrafish lens development. *Experimental*
557 *Eye Research*. DOI: 10.1016/j.exer.2013.09.007.

558 R Core Team. 2021.R: A language and environment for statistical computing. R Foundation for
559 Statistical Computing, Vienna, Austria. URL https://www.R-project.org/

560 R Studio Team. 2020. RStudio: Integrated Development for R. RStudio, PBC, Boston, MA URL
561 http://www.rstudio.com/

562 Smith AA, Wyatt K, Vacha J, Vihtelic TS, Zigler JS, Wistow GJ, Posner M. 2006. Gene duplication and
563 separation of functions in alphaB-crystallin from zebrafish (Danio rerio). *The FEBS journal* 273:481–
564 490. DOI: 10.1111/j.1742-4658.2005.05080.x.

565 Srinivasan AN, Nagineni CN, Bhat SP. 1992. alpha A-crystallin is expressed in non-ocular tissues. *The*
566 *Journal of biological chemistry* 267:23337–23341.

567 Vorontsova I, Gehring I, Hall JE, Schilling TF. 2018. Aqp0a Regulates Suture Stability in the Zebrafish
568 Lens. *Investigative ophthalmology & visual science* 59:2869–11. DOI: 10.1167/iovs.18-24044.

569 Wang K, Vorontsova I, Hoshino M, Uesugi K, Yagi N, Hall JE, Schilling TF, Pierscionek BK. 2020. Optical
570 development in the zebrafish eye lens. *FASEB journal : official publication of the Federation of*
571 *American Societies for Experimental Biology* 95:399–11. DOI: 10.1096/fj.201902607r.

572 Wu RS, Lam II, Clay H, Duong DN, Deo RC, Coughlin SR. 2018. A Rapid Method for Directed Gene
573 Knockout for Screening in G0 Zebrafish. *Developmental Cell* 46:112-125.e4. DOI:
574 10.1016/j.devcel.2018.06.003.

575 Zou P, Wu S-Y, Koteiche HA, Mishra S, Levic DS, Knapik E, Chen W, McHaourab HS. 2015. A conserved
576 role of αA-crystallin in the development of the zebrafish embryonic lens. *Experimental Eye Research*
577 138:104–113. DOI: 10.1016/j.exer.2015.07.001.

578

Figure 1

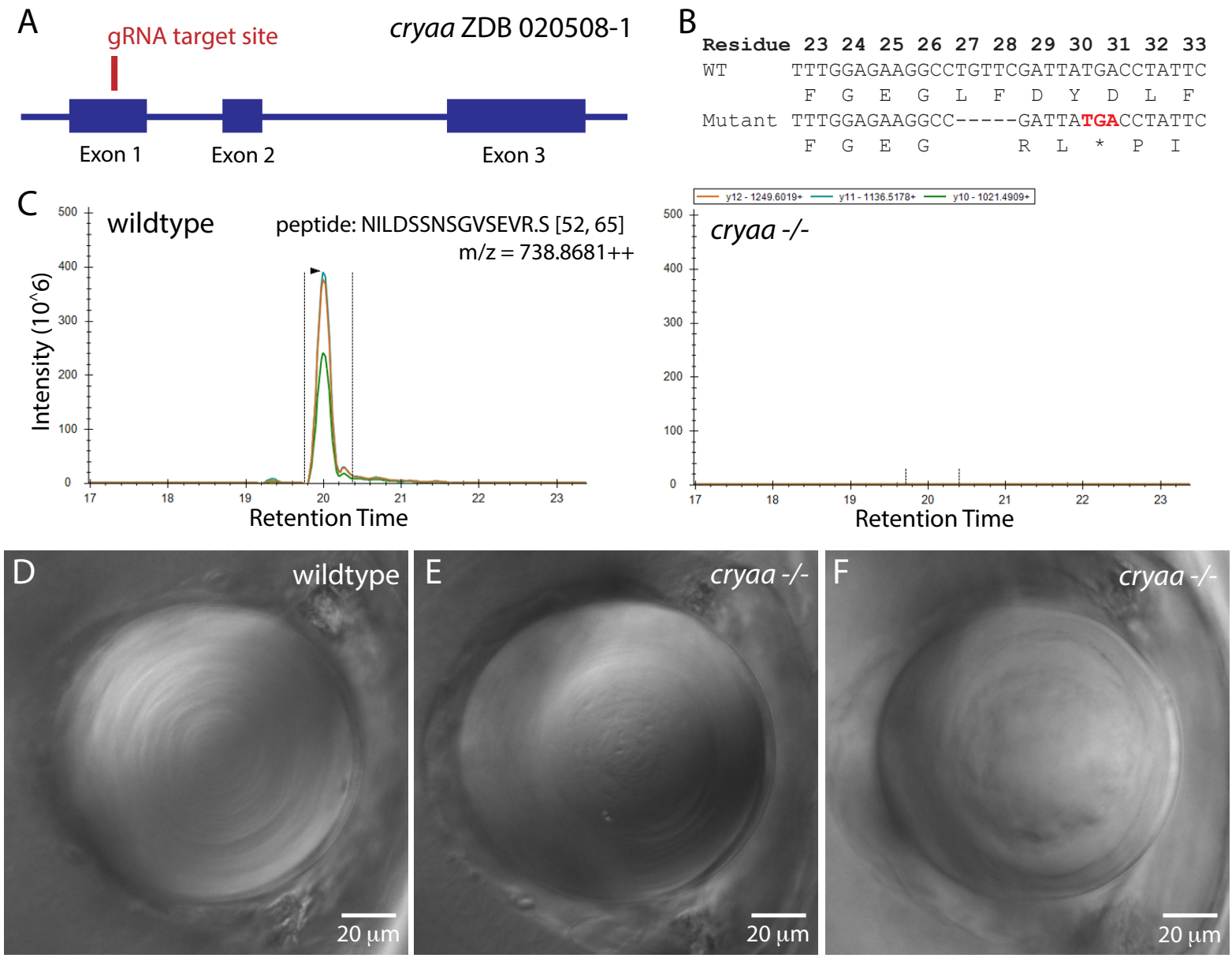

Figure 1. *cryaa* null mutant. Produced with a single gRNA to generate a five basepair deletion and frame shift mutation in exon 1, with relative position noted by red line (A). Injected embryos were outcrossed to wildtype fish to identify heterozygote mutants, with a five basepair deletion allele identified that leads to an early stop codon after amino acid 28 (B). Incrossed heterozygotes were used to generate a homozygous null line, which was bred to assess the effects of *cryaa* loss. Mass spectrometry confirmed that embryos generated by incrossing this null line produced no detectable alpha A crystallin protein (C). Parallel reaction monitoring of the 3 major fragment ions of the +3 charge state of *cryaa* peptide 52-65 from the digest of wildtype lenses showed coelution of its three major fragment ions on the left and no corresponding peaks in the digest from KO lenses on the right (C). Compared to wildtype lenses at 3 dpf (D), *cryaa* null embryos showed various defects such as roughness in the primary fiber cell region (E) and a general disorganization of central fiber cells (F). Lenses are from 3 dpf embryos, imaged using DIC optics and arranged with retina to the left. Scale bars are 20 microns.

Figure 2

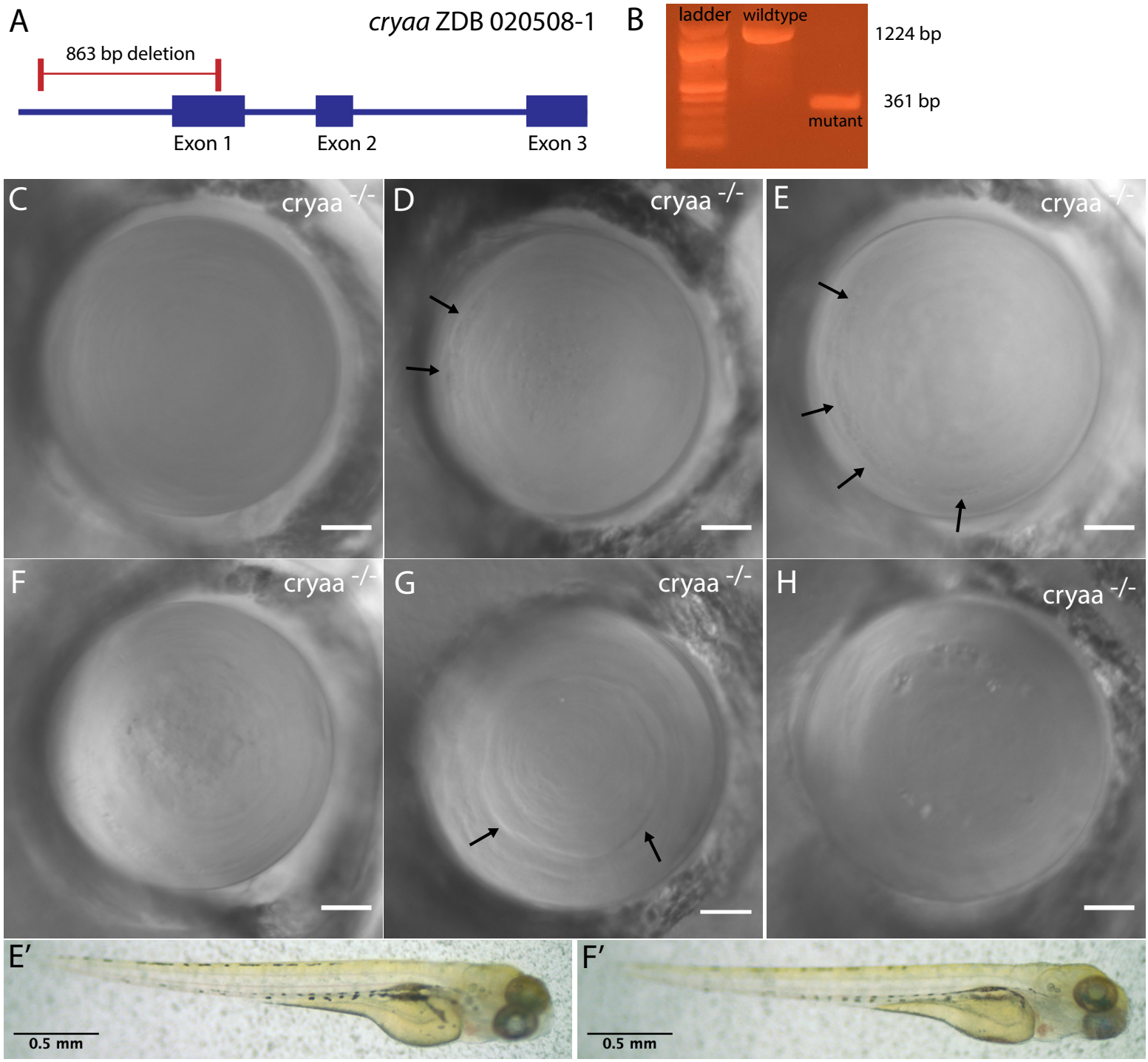

Figure 2. Second *cryaa* null mutant line generated by deleting start codon and proximal promoter region produced variable lens phenotypes. Two gRNAs were designed to remove approximately 860 basepairs of the *cryaa* gene (A). This large deletion could be easily identified using PCR amplification with primers flanking the gRNA target regions (B). Some *cryaa* null embryos showed visually normal lenses by DIC imaging (C). Typical phenotypes in abnormal lenses included roughness in central primary fiber cells (D), and general disorganization of central fiber cells (E), as seen in our single gRNA null mutant (Figure 1). Gaps or pits between peripheral fiber cells were also common (D and E: arrows). Some lenses combined several of these phenotypes (F). We also saw lenses with severe boundaries between fiber cells (G: arrows) and pitting (H). Lenses shown are either 3 or 4 dpf and arranged with retina to the left. Scale bars are 20 microns. Matching embryos for lenses E and F are shown to indicate lack of general morhological defects (E' and F').

Figure 3

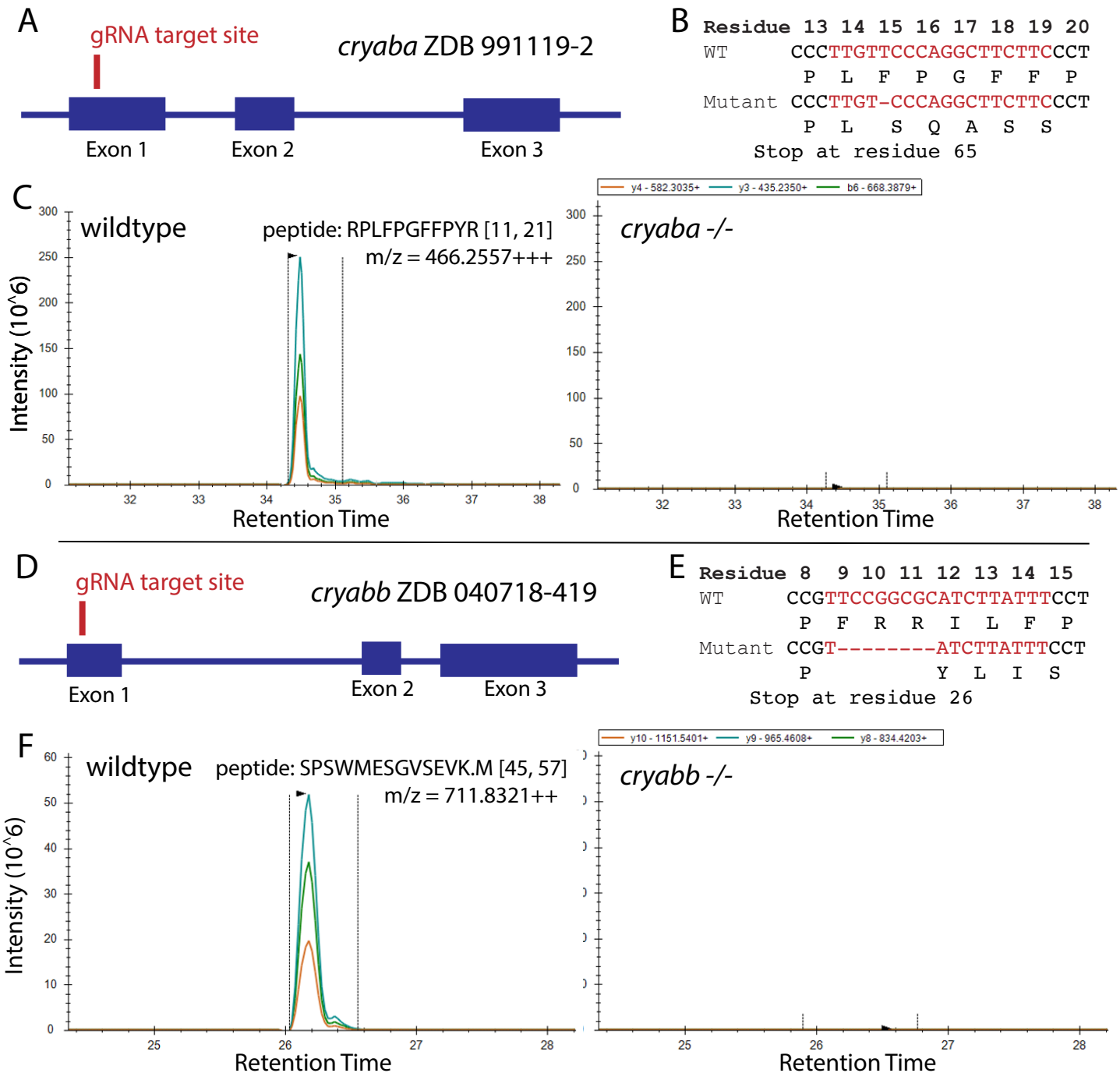

Figure 3. Production of *cryaba* and *cryabb* frameshift mutants. Single gRNAs were designed to target the first exons of the zebrafish *cryaba* (A) and *cryabb* (D) genes. After injection into wildtype zygotes founders were outcrossed to wildtype fish and resulting heterozygotes with deletions that caused frameshift mutations leading to early stop codons were detected (B and E). Mass spectrometry analysis of adult lenses from mutant null lines confirmed the loss of protein coded by each gene. Parallel reaction monitoring of the +3 charge state of αBa-crystallin tryptic peptide 11-21 from the digest of wildtype lenses detected coelution of its three major fragment ions (left) and these were not detectable in *cryaba* null adult lenses (C). Similarly, the +2 charge state of αBb-crystallin tryptic peptide 45-57 from the digest of wildtype lenses detected coelution of its three major fragment ions (left) and these were missing in digests from *cryabb* null adult lenses on the right (F).

Figure 4

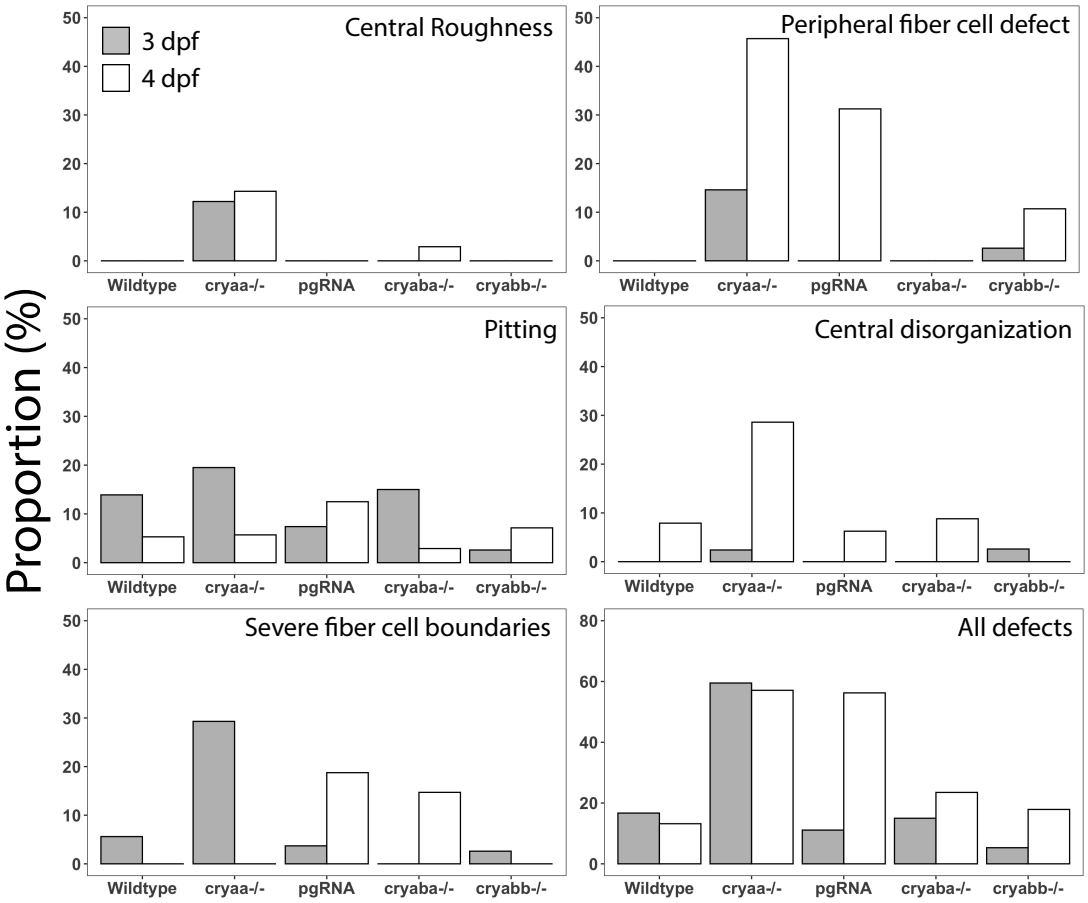

Figure 4. Prevalence of different lens abnormalities in wildtype, α-crystallin knockout and *cryaa* gRNA injected larvae at 3 and 4 dpf. Each graph shows the proportion of larvae with that defect type. Larvae examined at 3 and 4 dpf, respectively were wildtype (n= 36/38), offspring of homozygous null mutants for *cryaa* (n=41/35), *cryaba* (n=40/34) and *cryabb* (n=38/28), and embryos injected with a four-gRNA mix targeting the *cryaa* gene (pgRNA; n=27/16).

Figure 5

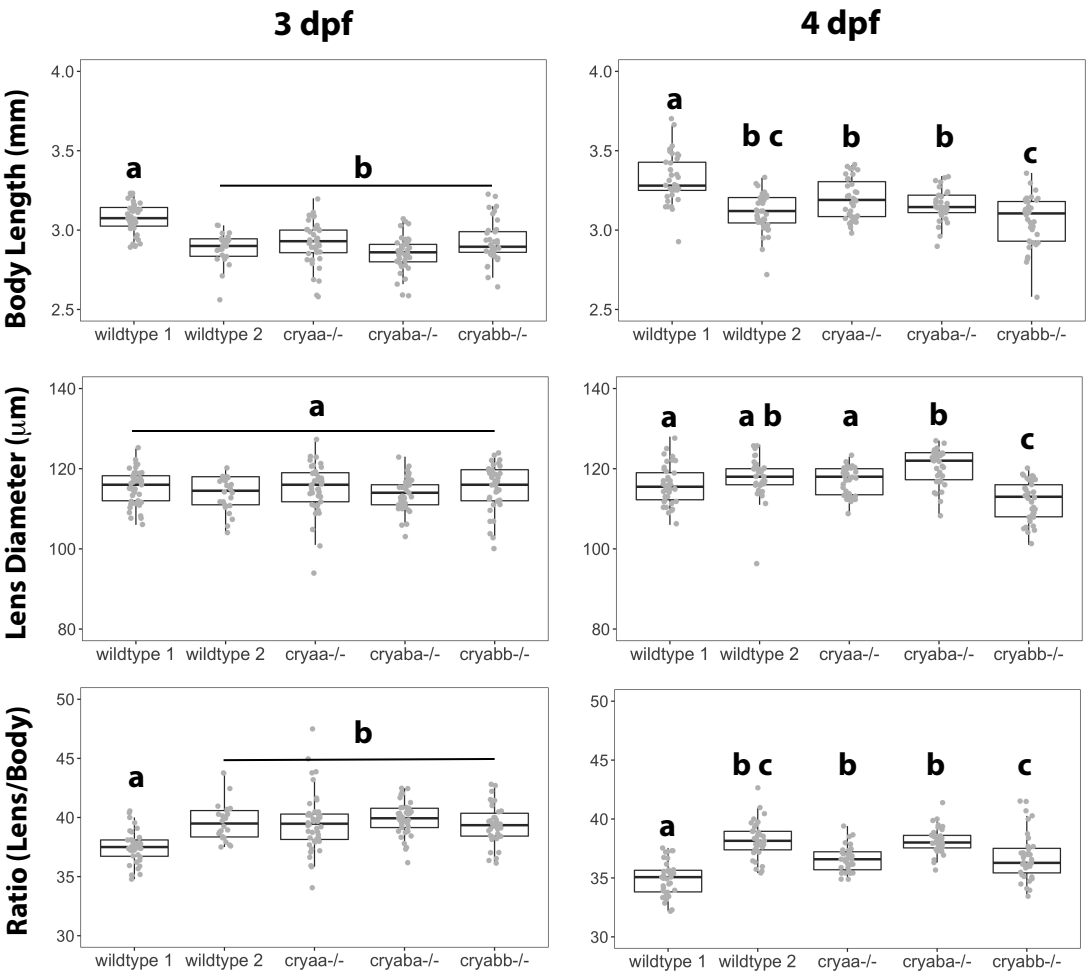

Figure 5. Comparison of lens diameters and body lengths between wildtype and α-crystallin knockout embryos. Box and whisker plots show measurements at 3 and 4 days post fertilization. Analysis of variance with Tukey post test was used to identify statistically significant differences between groups. Letters indicate statistical groups within each panel.

Figure 6

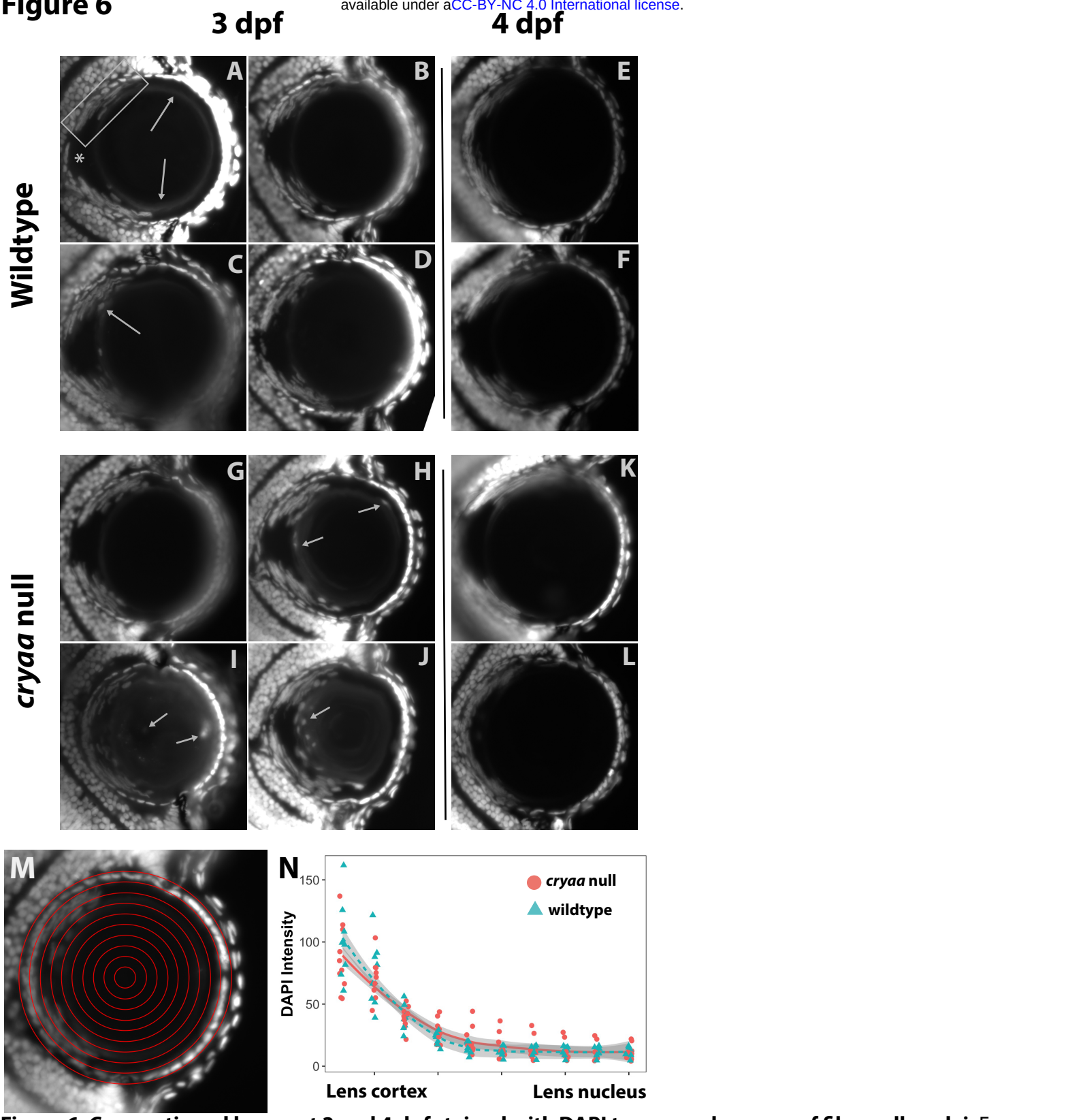

Figure 6. Cryosectioned lenses at 3 and 4 dpf stained with DAPI to assess clearance of fiber cell nuclei. Four representative lenses are shown for wildtype (A-D) and the *cryaa* null line (G-J) at 3 dpf, and two representative lenses at 4 dpf (E-F; K-L). Most images were taken at 200X total magnification, with some taken at 100X to capture more lens cell nuclei in one focal plane. Retina is oriented to the left in each image, with cornea to the right. The four images at 3 dpf for each genotype demonstrate the range of phenotypes found, with the top left panel the most normal and bottom right the most abnormal. Rectangle in panel A highlights one of two regions of flattened, extended fiber cell nuclei at retinal side of the lens, separated by a nucleus free zone at *. Arrows indicate details described in the results section. Concentric circles were used to measure average pixel density of DAPI staining across the lens (see M as an example). While some *cryaa* null lenses showed higher DAPI intensity in inner areas of the lens at 3 dpf (N), these differences were not statistically significant (Mann-Whitney U test).

Figure 7

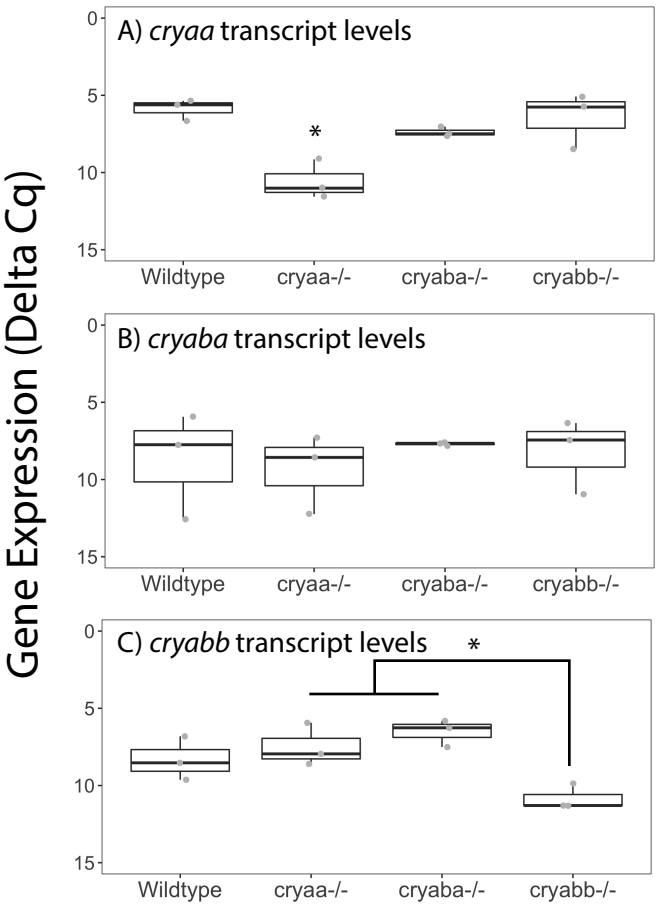

Figure 7. Expression of each α-crystallin gene assayed by qPCR in whole bodies of wildtype and mutant larvae at 7 dpf. Box and whisker plots show delta Cq values generated with primers for *cryaa* (A), *cryaba* (B) and *cryabb* (C) in three biological replicates of the genotypes indicated on the x-axes. Y-axes are inverted as lower delta Cq values indicate greater expression. Asterisks indicate statistically significant differences based on ANOVA with Tukey post test (*p-value* < 0.05).